Electronic Supplementary Material (ESI) for Journal of Materials Chemistry C.

Boosting PEDOT energy storage with redox anthraquinone dopant for flexible hydrogel supercapacitor under sub-zero temperatures

Chen Chen[a,b], Yueqin Li[a,b]*, Changhao Qian[a,b], Xiaohui Liu[a,b], Yong Yang[a,b], Lin Han[b]

[a]Jiangsu Co-Innovation Center of Efficient Processing and Utilization of Forest Resources, Nanjing Forestry University, Nanjing 210037, China

[b]College of Chemical Engineering, Jiangsu Key Lab for the Chemistry & Utilization of Agricultural and Forest Biomass, Nanjing Forestry University, Nanjing 210037, China

*Corresponding Authors: Dr. Yueqin Li, E-mail: yueqinli@njfu.edu.cn; ORCID: 0000-0002-1991-0261.

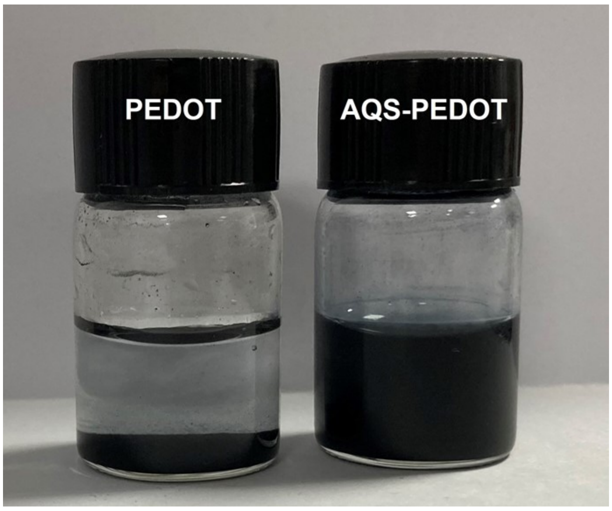

Figure S1. The dispersion properties of PEDOT and AQS-PDOT (1:5) in aqueous solutions (10 mg/mL) after an aging time of a week.

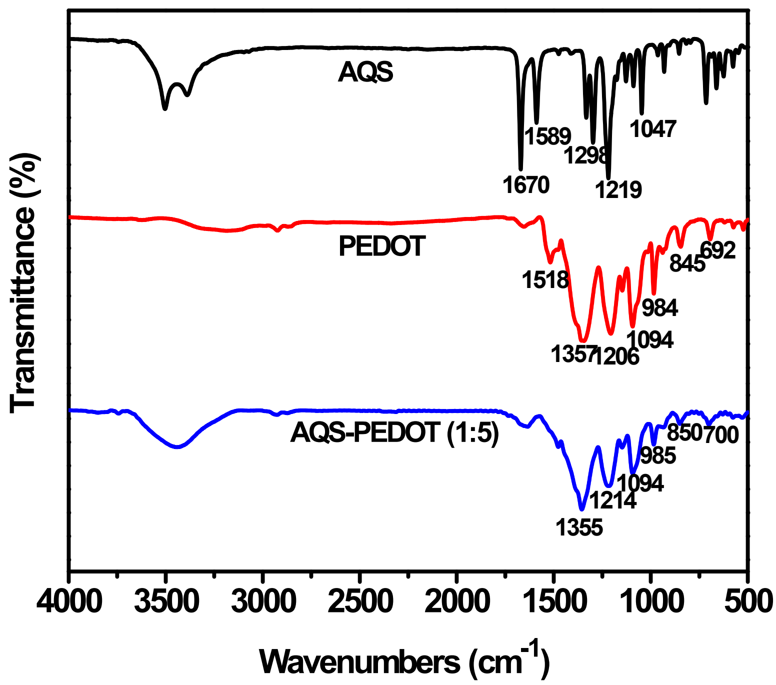

Figure S2. FTIR spectrum of the AQS, PEDOT and AQS-PEDOT (1:5) complex.

In the FTIR spectrum of the AQS, the peaks at 1670, 1589, 1298, 1219 and 1047 cm^{-1} are associated with C=O stretching, C=C stretching, C-C stretching, and the SO_3^- characteristic vibrations [1], respectively. The main characteristic peaks of PEDOT appeared at 1518 cm^{-1} (C=C stretching), 1357 cm^{-1} (C-C stretching), 1206 and 1094 cm^{-1} (C-O-C vibration), and finally 984, 845 and 692 cm^{-1} (C-S-C), which are all present in the FTIR spectrum of AQS-PEDOT (1:5) complex. In addition, the characteristic peak of the SO_3^- group was also observed in the AQS-PEDOT (1:5) complex. However, this peak showed a slight red-shift from 1219 to 1214 cm^{-1}; meanwhile this peak got broader, properly caused by merging of the bands of the C-O-C groups of the PEDOT moiety. Also, the characteristic of C-S stretching at 850 and 700 cm^{-1} have shifted to higher wavenumbers in comparison to pure PEDOT. This shift is related to interaction between positively charged PEDOT and negatively charged

AQS. Therefore, it is concluded that EDOT has gone through a complete oxidization process and successfully doped with AQS.

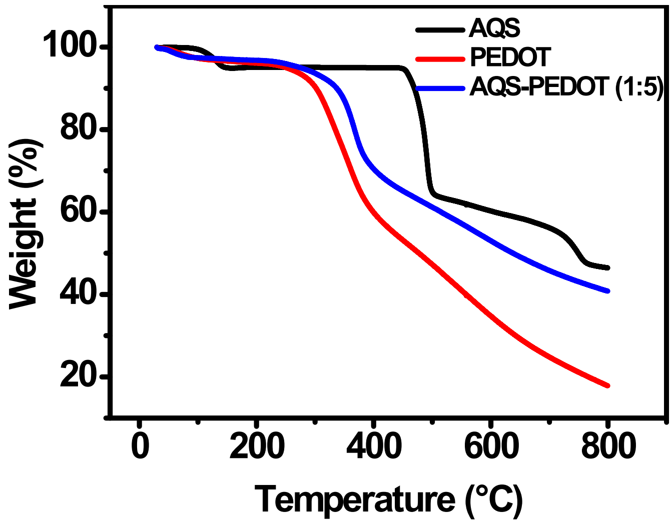

Fig. S3. TGA curves of raw AQS, PEODT, and AQS-PEDOT (1:5).

Fig. S3 shows the TGA results for quantitatively evaluating the doping degree of the AQS with PEDOT. In the TGA curves, a small amount of weight loss below 100 °C could be due to the removal of the adsorbed water. The raw AQS did not exhibit detectable weight loss up to 414 °C. The PEDOT The PEDOT and the AQS-PEDOT nanocomposite showed a similar TGA curve shape, indicating that a similar degradation procedure happened. They both had a huge weight loss from 200~400 °C. Note that AQS was stable in this temperature range, the amount of the PEDOT in the AQS-PEDOT nanocomposite can be calculated by the residual amounts of PEDOT and AQS-PEDOT at 400 °C of 59.86% and 70.45 %, respectively. Since the residue of AQS at the temperature of 400 °C was of 94.96%, the amount of PEDOT in the AQS-PEDOT can be calculated to be 69.98 wt%. This value was close to the amount of the EDOT monomers added into the AQS solution (68.40 wt%) during the preparation, confirming the high yield of the double oxidative polymerization of PEDOT.

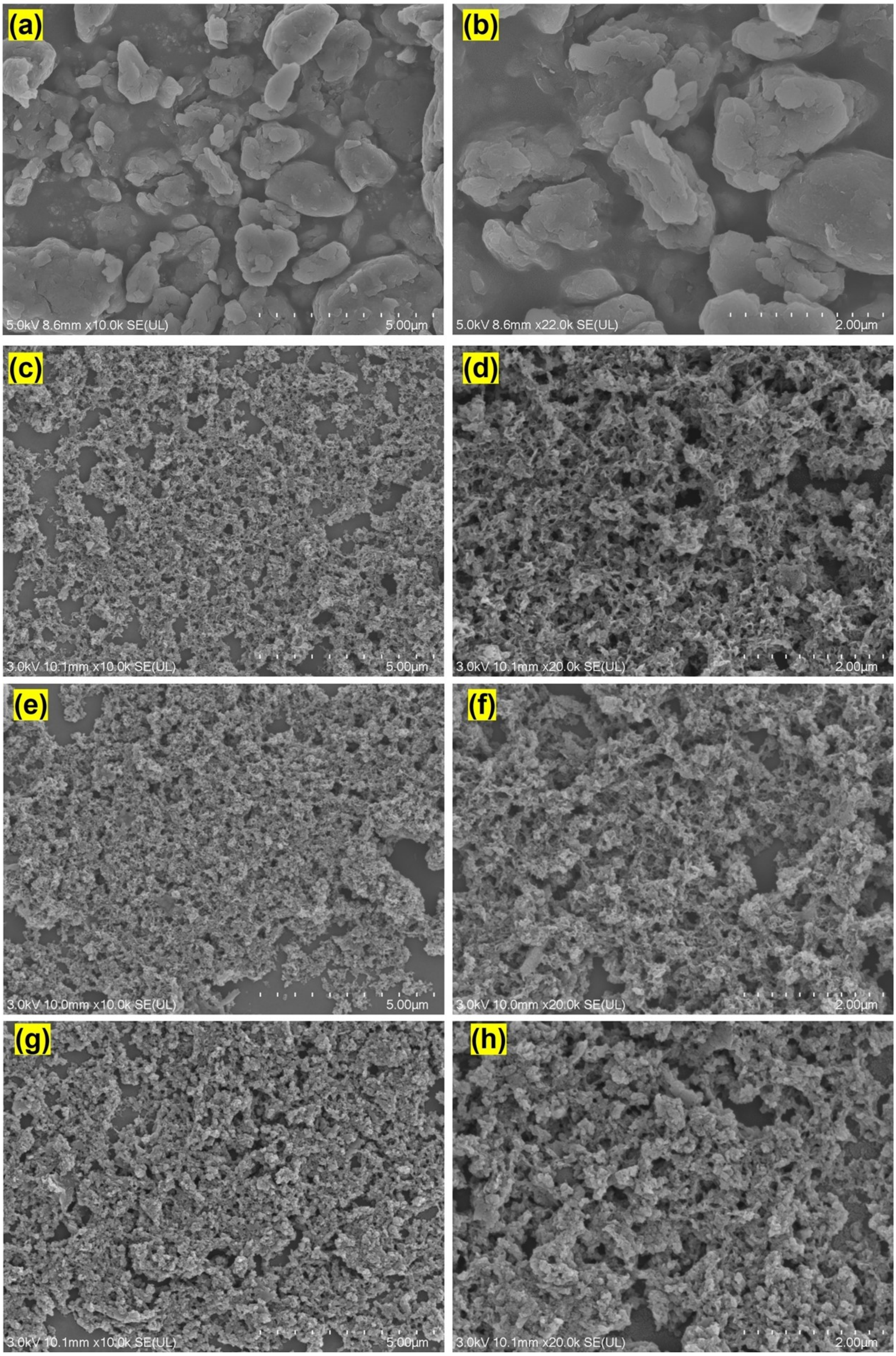

Fig. S4. SEM images of AQS-PEDOT conductive fillers with different feeding ratios of dopants (a, b) 1:7, (c, d) 1:5, and (e, f) 1:3.

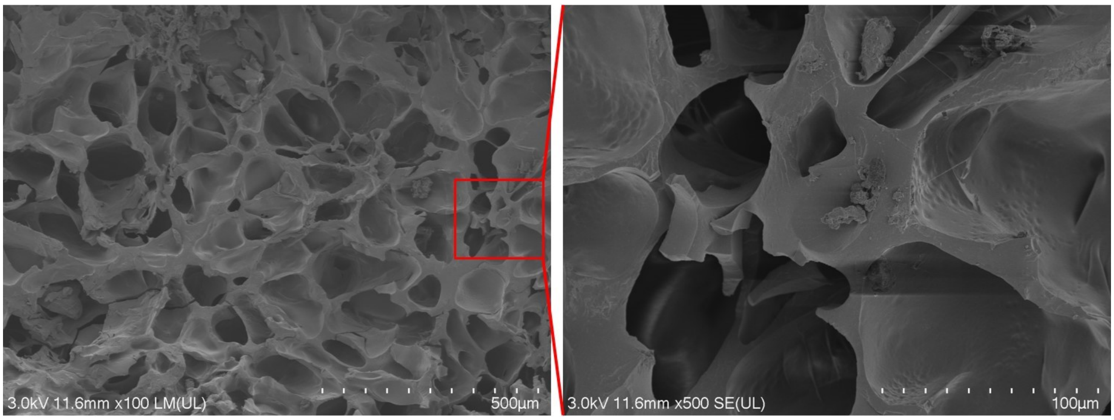

Fig. S5. SEM images of PEDOT/PAA hydrogel. Left, PEDOT/PAA hydrogel. Right, magnified image of circled area in PEDOT/PAA hydrogel.

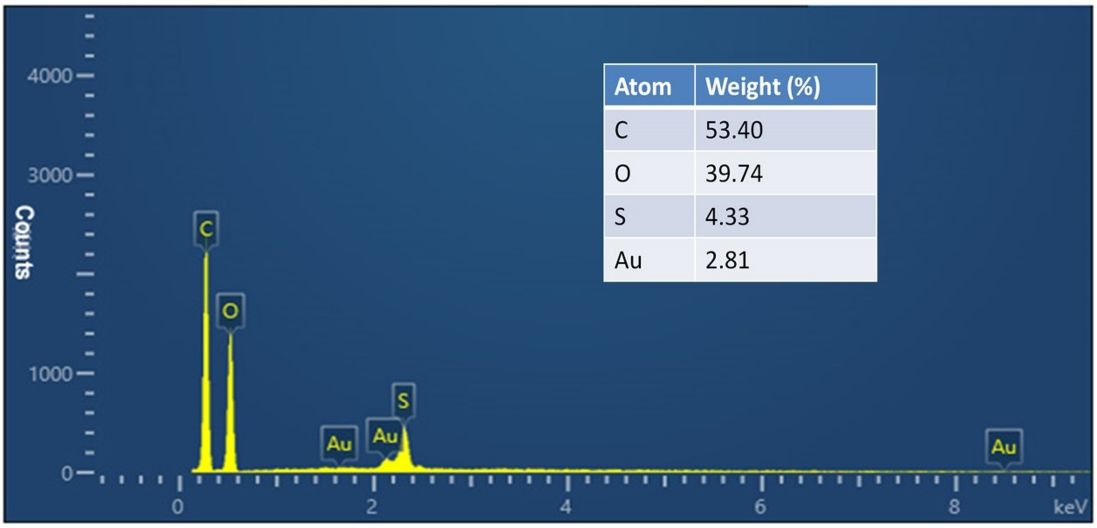

Fig. S6. EDS spectrum of the AQS-PEDOT/PAA electrode and the atom weight percentage.

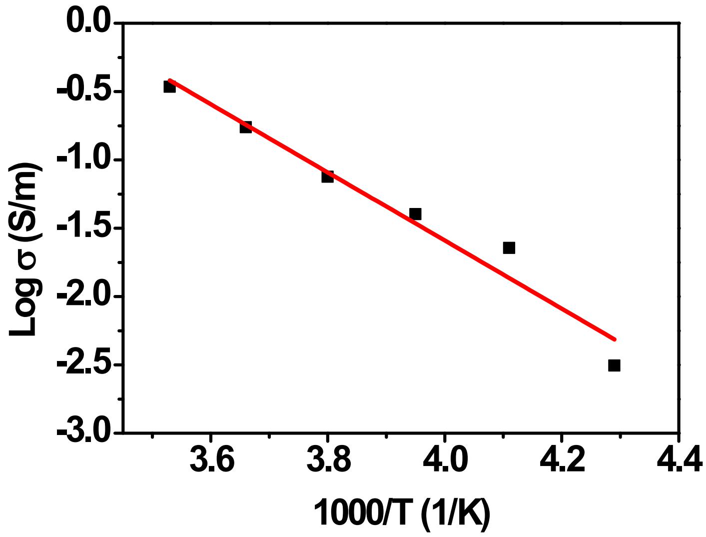

Fig. S7. Arrhenius plot of AQS-PEDOT/PAA hydrogel film.

$$\sigma = A\,exp(-\frac{E_a}{RT}) \qquad \text{Eq. S1}$$

where A is the pre-exponential, E_a is the activation energy (kJ/mol), R is the universal gas constant (J/(mol·K)), and T is the absolute temperature (K).

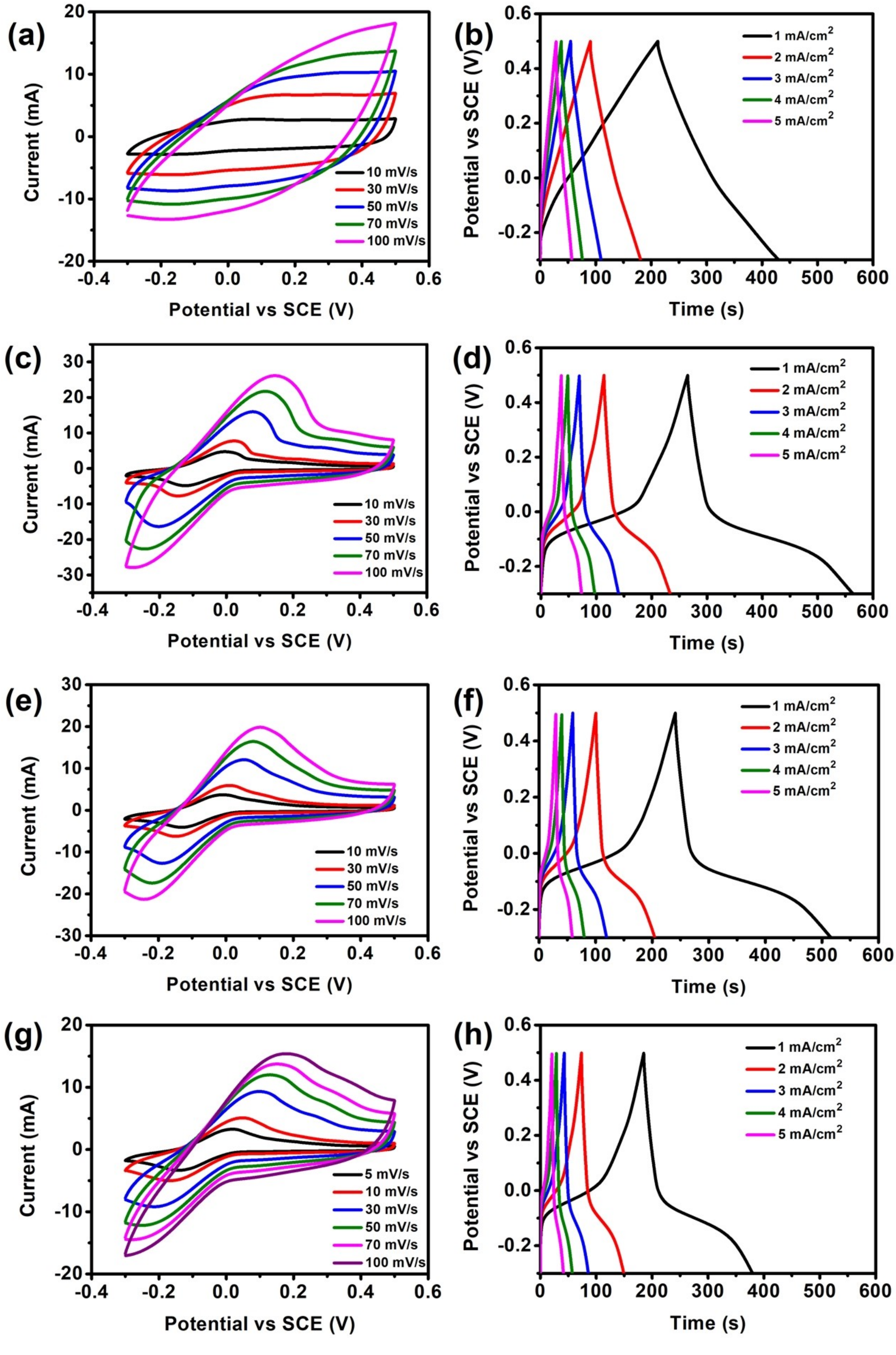

Fig. S8. CV and GCD curves of PEDOT/PAA electrode (a, b) and AQS-PEDOT/PAA electrodes with different feeding ratios of dopants (c, d) 1:7, (e, f) 1:3 and 1:2 (g, h), respectively.

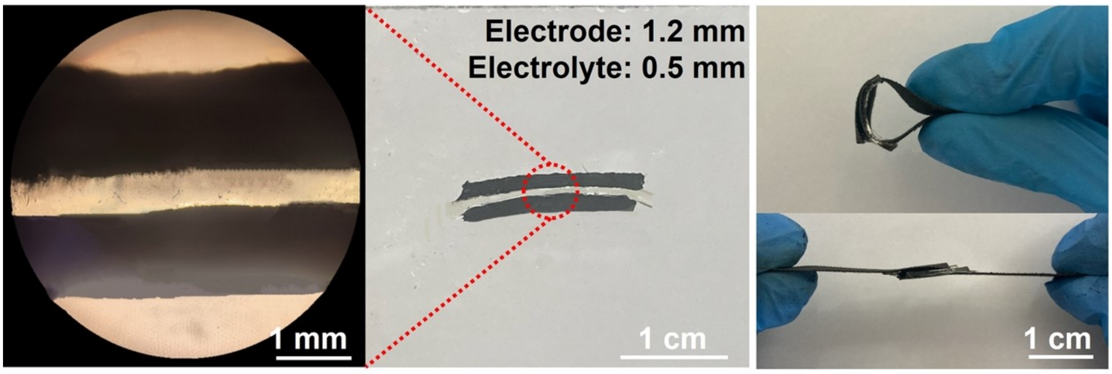

Fig. S9. The configuration of the assembled asymmetric SCs.

Table S1 Comparison of the electrochemical performance of reported advanced hydrogel supercapacitors with this work.

Electrode	C_a (mF/cm^2)	E_a (μWh/cm^2)	P_a (μW/cm^2)	Cyclic stability	Ref.
CNT+PEDOT:PSS/PAM+SA	128 (1 mA /cm^2)	3.6	200	80% (5000)	[2]
PEDOT:PSS/PVA/PMAA	7.38 (10 mV/s)	0.65	170	82%(2000)	[3]
CMC-PEDOT/PAAM	269 (1 mA /cm^2)	23.93	400	88% (5000)	[4]
PEDOT:PSS/PVA	128.9 (0.5 mA /cm^2)	11.46	200.5	89.8% (10000)	[5]
PPy/B-PVA/KCl	224 (0.8 mA/cm^2)	20	600	92% (1000)	[6]
PANI-PCH	488 (0.2 mA/cm^2)	42	1600	~100% (10000)	[7]
PANI-CNTP/PM	158.4 (0.01 mA)	14.08	285.71	-	[8]
CNT-PPy-PAA	0.22 (5 mV/s)	-	-	-	[9]
PANI-PHP	58.8 (0.2 mA/cm^2)	6.94	500	97% (10000)	[10]
PVA-CNM-PANI	286.4 (5 mV/s)	-	-	80% (5500)	[11]
PANI/PAAm	137.4 (0.5 mA/cm^2)	-	-	82% (2000)	[12]
PPy/CPH	261.2 (5 mA cm^{-2})	23.0	80	86.3% (10000)	[13]
MXene/PVA-H_2SO_4	328 (2 mV/s)	7.3	132		[14]
2DMON/CNTS	285 (2 mV/s)	14.2	940	80% (8000)	[15]
PAD/H_2SO_4-PANI	430 (0.5 mA cm^{-2})	22	150	90% (10000)	[16]
PVA/PHEA/PANI	98 (0.2 mA/cm^2)	8.48	78.52	98% (8000)	[17]
AQS-PEDOT/PAA	466.5 (1 mA cm^{-2})	41.47 27.56	400 4000	90% (5000)	This work

Table S2 Comparisons of temperature-tolerance of the AQS-PEDOT/PAA SC with the previously reported hydrogel SCs.

Sample	Temperature tolerance	Mechanical performance	Ref.
SA-g-DA/KCl electrolyte	-10 °C ~RT	elongation ~300%	[18]
MMT/PVA electrolyte	−50~90 °C	elongation ~22.6%	[19]
PVAPB electrolyte	−5~60 °C	-	[20]
PVA DN electrolyte	-40 °C ~RT	Compression strain ~60%	[21]
SA–borax/gelatin electrolyte	−20~60 °C	elongation 305.7%	[22]
MGO-PAM electrolyte	-30~100 °C	~ 480% extension ratio	[23]
PAM-PVP semi-IPN electrolyte	−20~RT	elongation ~1600%	[24]
P(AMPS$_{0.3}$-co-AAM$_{0.4}$) electrolyte	−20 to 100 °C	Strain 900%	[25]
PCH/AV_FS//PANI SC	-40 °C ~RT	~ 500% extension ratio	[26]
AQS-PEDOT/PAA SC	-30~90 °C	Strain 1180%	This work

RT represents room temperature; – means not available.

References

[1] L. Zhang, D. Han, Y. Tao, C. Cui, Y. Deng, X. Dong, W. Lv, Z. Lin, S. Wu, Z. Weng, Q.-H. Yang, Dense organic molecules/graphene network anodes with superior volumetric and areal performance for

asymmetric supercapacitors, J. Mater. Chem. A, 8 (2020) 461-469.
[2] J. Zeng, L. Dong, W. Sha, L. Wei, X. Guo, Highly stretchable, compressible and arbitrarily deformable all-hydrogel soft supercapacitors, Chemical Engineering Journal, (2019) 123098.
[3] C.-C. Shih, Y.-C. Lin, M. Gao, M. Wu, H.-C. Hsieh, N.-L. Wu, W.-C. Chen, A rapid and green method for the fabrication of conductive hydrogels and their applications in stretchable supercapacitors, J. Power Sources, 426 (2019) 205-215.
[4] C. Chen, Y. Li, C. Qian, X. Liu, Y. Yang, L. Han, Q. Han, Carboxymethyl cellulose assisted PEDOT in polyacrylamide hydrogel for high performance supercapacitors and self-powered sensing system, European Polymer Journal, 179 (2022) 111563.
[5] Q. Liu, J. Qiu, C. Yang, L. Zang, G. Zhang, E. Sakai, High-Performance PVA/PEDOT:PSS Hydrogel Electrode for All-Gel-State Flexible Supercapacitors, Adv. Mater. Technol., 6 (2021) 2000919.
[6] K. Sun, E. Feng, G. Zhao, H. Peng, G. Wei, Y. Lv, G. Ma, A Single Robust Hydrogel Film Based Integrated Flexible Supercapacitor, ACS Sustainable Chemistry & Engineering, 7 (2019) 165-173.
[7] K. Wang, X. Zhang, C. Li, X. Sun, Q. Meng, Y. Ma, Z. Wei, Chemically Crosslinked Hydrogel Film Leads to Integrated Flexible Supercapacitors with Superior Performance, Adv. Mater., 27 (2015) 7451-7457.
[8] L. Chen, Z. Gu, L. Li, W. Lei, Q. Rong, C. Zhao, Q. Wu, Z. Gu, X. Jin, L. Jiang, M. Liu, Integration of hydrogels with functional nanoparticles using hydrophobic comb-like polymers as an adhesive layer, J. Mater. Chem., 6 (2018) 15147-15153.
[9] M. Hu, J. Wang, J. Liu, J. Zhang, X. Ma, Y. Huang, An intrinsically compressible and stretchable all-in-one configured supercapacitor, Chem. Commun., 54 (2018) 6200-6203.
[10] B.-S. Yin, S.-W. Zhang, K. Ke, Z.-B. Wang, Advanced deformable all-in-one hydrogel supercapacitor based on conducting polymer: Toward integrated mechanical and capacitive performance, J. Alloys Compd., 805 (2019) 1044-1051.
[11] R. Hu, Y. Wang, J. Zhao, R. Jiang, J. Zheng, Fabrication of stretchable multi-element composite for flexible solid-state electrochemical capacitor application, Chemical Engineering Journal, 361 (2019) 109-116.
[12] H. Wang, L. Dai, D. Chai, Y. Ding, H. Zhang, J. Tang, Recyclable and tear-resistant all-in-one supercapacitor with dynamic electrode/electrolyte interface, J. Colloid Interface Sci., 561 (2020) 629-637.
[13] L. Zang, Q. Liu, J. Qiu, C. Yang, C. Wei, C. Liu, L. Lao, Design and Fabrication of an All-Solid-State Polymer Supercapacitor with Highly Mechanical Flexibility Based on Polypyrrole Hydrogel, ACS Appl Mater Interfaces, 9 (2017) 33941-33947.
[14] M. Hu, Z. Li, G. Li, T. Hu, C. Zhang, X. Wang, All-Solid-State Flexible Fiber-Based MXene Supercapacitors, Adv. Mater. Technol., 2 (2017) 1700143.
[15] H. Yu, N. Rouelle, A. Qiu, J.-A. Oh, D.M. Kempaiah, J.D. Whittle, M. Aakyiir, W. Xing, J. Ma, Hydrogen Bonding-Reinforced Hydrogel Electrolyte for Flexible, Robust, and All-in-One Supercapacitor with Excellent Low-Temperature Tolerance, ACS Appl. Mater. Interfaces, 12 (2020) 37977-37985.
[16] Y. Shi, Y. Zhang, L. Jia, Q. Zhang, X. Xu, Stretchable and Self-Healing Integrated All-Gel-State Supercapacitors Enabled by a Notch-Insensitive Supramolecular Hydrogel Electrolyte, ACS Appl. Mater. Interfaces, 10 (2018) 36028-36036.
[17] J. Yang, X. Yu, X. Sun, Q. Kang, L. Zhu, G. Qin, A. Zhou, G. Sun, Q. Chen, Polyaniline-Decorated Supramolecular Hydrogel with Tough, Fatigue-Resistant, and Self-Healable Performances for All-In-

One Flexible Supercapacitors, ACS Applied Materials & Interfaces, 12 (2020) 9736-9745.
[18] F. Tao, L. Qin, Z. Wang, Q. Pan, Self-Healable and Cold-Resistant Supercapacitor Based on a Multifunctional Hydrogel Electrolyte, ACS Appl. Mater. Interfaces, 9 (2017) 15541-15548.
[19] C. Lu, X. Chen, All-Temperature Flexible Supercapacitors Enabled by Antifreezing and Thermally Stable Hydrogel Electrolyte, Nano Lett., 20 (2020) 1907-1914.
[20] W. Lv, R. Xue, S. Chen, M. Jiang, Temperature stability of symmetric activated carbon supercapacitors assembled with in situ electrodeposited poly(vinyl alcohol) potassium borate hydrogel electrolyte, Chin. Chem. Lett., 29 (2018) 637-640.
[21] Z. Liu, J. Zhang, J. Liu, Y. Long, L. Fang, Q. Wang, T. Liu, Highly compressible and superior low temperature tolerant supercapacitors based on dual chemically crosslinked PVA hydrogel electrolytes, J. Mater. Chem. A, 8 (2020) 6219-6228.
[22] K. Peng, J. Zhang, J. Yang, L. Lin, Q. Gan, Z. Yang, Y. Chen, C. Feng, Green Conductive Hydrogel Electrolyte with Self-Healing Ability and Temperature Adaptability for Flexible Supercapacitors, ACS Appl. Mater. Interfaces, 14 (2022) 39404-39419.
[23] X. Jin, G. Sun, G. Zhang, H. Yang, Y. Xiao, J. Gao, Z. Zhang, L. Qu, A cross-linked polyacrylamide electrolyte with high ionic conductivity for compressible supercapacitors with wide temperature tolerance, Nano Res., 12 (2019) 1199-1206.
[24] M. Wang, L. Fan, G. Qin, X. Hu, Y. Wang, C. Wang, J. Yang, Q. Chen, Flexible and low temperature resistant semi-IPN network gel polymer electrolyte membrane and its application in supercapacitor, J. Membr. Sci., 597 (2020) 117740.
[25] Y. Liu, H. Li, X. Wang, T. Lv, K. Dong, Z. Chen, Y. Yang, S. Cao, T. Chen, Flexible supercapacitors with high capacitance retention at temperatures from −20 to 100 °C based on DMSO-doped polymer hydrogel electrolytes, J. Mater. Chem. A, 9 (2021) 12051-12059.
[26] G. Qin, Y. Liu, W. Zhang, W. He, X. Su, Q. Lv, X. Yu, Q. Chen, J. Yang, Integrated supercapacitor with self-healing, arbitrary deformability and anti-freezing based on gradient interface structure from electrode to electrolyte, J. Colloid Interface Sci., 635 (2023) 427-440.